



The influence of process parameters on the preparation of closed-cell aluminum foam by friction stir processing

Qiu Pang^{1,2,3} · Zhengjian Wu³ · Zhili Hu³

Received: 18 July 2021 / Accepted: 15 February 2022 / Published online: 23 February 2022
© The Author(s), under exclusive licence to Springer-Verlag London Ltd., part of Springer Nature 2022

Abstract

In order to obtain high-quality aluminum foam components, a new preparation method for a 7075 closed-cell aluminum foam based on friction stir processing (FSP) was proposed. The influence of process parameters on microstructures of closed-cell Al foam precursor was investigated by optical metallographic microscope and scanning electronic microscope (OM/SEM). The temperature field and flow field of the Al foam precursor during FSP were simulated by Fluent CFD software. The formability of the Al foam precursor was analyzed by the cupping test. It is found that the rotating speed has great influence on the uniformity and density of the precursor prepared by FSP, but the welding speed has little influence. Numerical simulation shows that the maximum flow velocity of material in the tool shoulder increases by 1.5 times when the rotating speed increases from 800 to 2000 r/min, and the peak temperature at the stirring pin reaches 491 °C, which is consistent with the experimental results. The powder ring is continuous and uniform due to sufficient plastic deformation and flow at travel speed of 50 mm/min and the rotating speed of 2000 r/min. The formability of the precursor increases with the increase of deformation temperature. Especially the cupping test value of precursor is close to that of base metal at 450 °C. In the foaming process, the foam pores first appear at the bottom and then expand upwards with the extension of the foaming time. The expansion rate of the whole foam increases rapidly, and the pores with highly spherical are homogeneously distributed when the foaming time is 110 s at 680 °C.

Keywords Aluminum foam · Friction stir processing · Numerical simulation · Microstructure

1 Introduction

Aluminum foams are a new integrated functional material with unique structure and properties [1–3]. Compared to solid metals, they hold excellent properties such as light weight, large specific surface area, high specific strength, low effective thermal conductivity and high-energy

absorption performance. Therefore, they may be used in aerospace, automobile transportation, military, and marine industries [4, 5]. In particular, closed-cell aluminum foams are of increasing importance because of their energy absorption capabilities, combined with good mechanical properties and low density. The current preparation methods of aluminum foam include powder metallurgy, direct gas foaming, and casting technique. However, aluminum foams prepared by these methods have low toughness and strength. The foam pore is easy to collapse after deformation. The application scope of aluminum foam structural parts is greatly limited, which is mainly applied to flat components [6–10].

Friction stir welding (FSW) is a new and innovative solid-state joining process, which generates intense plastic deformation. FSW has proven very successful in creating high quality welds for a wide range of materials [11–13]. Its advantages include low shrinkage, fewer defects, low welding temperature, and excellent mechanical properties. Especially, FSW has been recognized as a very practicable joining process for 2000 and 7000 Al alloys [14], which

✉ Zhili Hu
zhilihuhit@163.com

¹ Key Laboratory of Metallurgical Equipment and Control Technology of Ministry of Education, Wuhan University of Science and Technology, Wuhan 430081, People's Republic of China

² Hubei Key Laboratory of Mechanical Transmission and Manufacturing Engineering, Wuhan University of Science and Technology, Wuhan 430081, People's Republic of China

³ Hubei Key Laboratory of Advanced Technology for Automotive Components, Wuhan University of Technology, Wuhan 430070, People's Republic of China

Table 1 Chemical composition of 7075-O aluminum alloy (wt.%)

Type	Element								
	Zn	Mg	Cu	Mn	Si	Fe	Cr	Ti	Al
7075-O	5.0–6.2	2.0–2.8	1.1–2.0	0.29	0.41	0.49	0.19–0.27	0.20	Balance

are difficult to fusion welded. Many studies have confirmed that the weld strength and toughness after FSW is obviously higher than that of corresponding fusion welds.

In recent years, a FSP route as a surface-modifying technique has been investigated to modify microstructures and their properties through high strain rate deformation [15, 16]. FSP is developed from the basic principles of FSW. The FSP has made some achievements in the research of particle reinforced aluminum matrix composites. The dispersion of reinforced particles in Al matrix increases as the number of FSP passes increase. At present, FSP with an enormous potential has been developed to fabricate the precursor of Al foam [17–19]. The stabilization agent powder can be mixed into the die casting plates to fabricate the precursor by intense plastic deformation and stirring of tool. Then, the porous aluminums are successfully obtained by post-weld foam treatment [20, 21]. However, till to present, the effects of process parameters on microstructures of closed-cell Al foam precursor are not analyzed in detail. Numerical studies on the flow field and temperature field in FSP are not effectively combined.

In this study, in order to obtain high-quality aluminum foam components by FSP, the characteristics of microstructure, the temperature distribution and material flow near the stirring pin during the preparation of Al foam are revealed by experimental and numerical methods. The effects of different process parameters on microstructure, temperature distribution, and material flow of the Al foams are evaluated. The Fluent CFD software is used to solve the numerical simulation in FSP. Simultaneously, the tracking particles and heat transfer during the FSP are analyzed. The cupping test of Al foam precursor is also carried out. The effects of deformation temperature and the number of FSP passes on the bulging properties of Al foam precursor are investigated.

2 Experimental procedure

The 7075-O aluminum alloy plate of 200 mm×100 mm×1.5 mm sizes were used to prepare aluminum foam precursor by FSP, and its main chemical composition was shown in Table 1. The closed-cell Al foams were prepared by 3 FSP passes. The foaming agent was TiH₂ powder with particle size of 45 μm. The stabilizer was Al₂O₃ powder with particle size of 1 μm. The photograph of FSP equipment is shown in Fig. 1. FSP was carried out with a tool made of 4Cr5MoV steel. The shoulder diameter of the tool was 24 mm. The pin diameter was 5 mm and the pin height was 2.85 mm in Fig. 2.

At first, the 1 wt% TiH₂ and 2 wt% Al₂O₃ powder were mixed with the planetary ball mill at a speed of 250 rpm for 90 min. Then, the mixed powders were spread evenly between two 7075-O aluminum alloy plates. The schematic illustrations of closed-cell Al foam precursor by multipass FSP is shown in Fig. 3. The different travel speeds (50, 100, and 200 mm/min) and rotation speeds (800, 1200, 1600, and 2000 r/min) were used for multipass FSP. The number of welding was 3 passes, and the welding spacing was 3 mm. The length of passes was 240 mm in each case. The samples were cut into 20 mm×20 mm by line cutting machine, and then the polished samples were etched with Keller's reagent (1 ml HF + 1.5 ml HCl + 2.5 ml HNO₃ + 95 ml H₂O). The precursors were foamed by using a heat treatment furnace. According to the literature [20], the foaming temperature was selected as 680 °C.

The microstructure of closed-cell Al foam and the distribution of TiH₂ and Al₂O₃ powder in the matrix were analyzed by optical metallographic microscope (OM) and scanning electron microscope (SEM/EDS), respectively. The influences of different process parameters on the morphology of closed-cell Al foams were investigated in

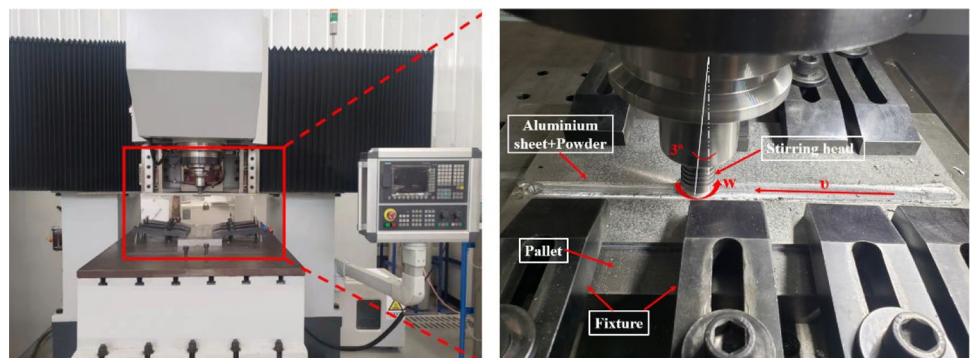
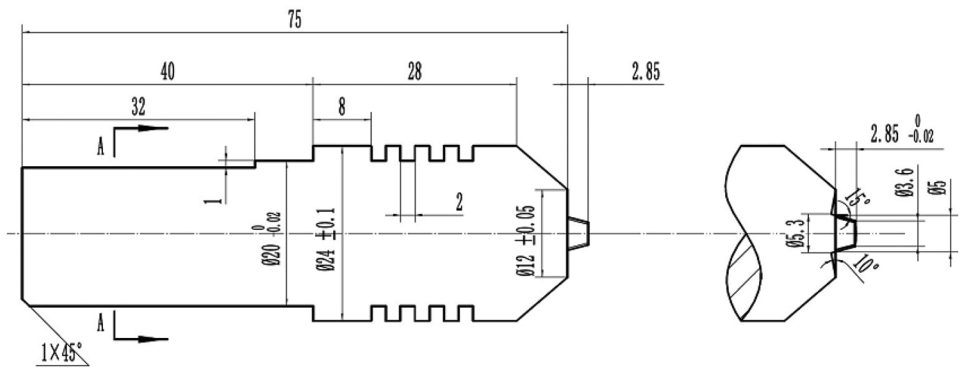
Fig. 1 The photograph of FSP equipment

Fig. 2 FSP tool geometry



detail. In addition, the cupping test of Al foam precursor was completed in an electric furnace equipped with a thermocouple. The deformation temperatures were measured by thermocouple. The experiment was carried out by using the servo pressure test system. The test conditions included the sample size for 90 mm diameter, deformation speed 5 mm/s, and deformation temperature (25 °C, 300 °C, 400 °C, 450 °C, 475 °C). The effects of deformation temperature on the bulging properties of Al foam precursor were analyzed in detail.

3 Numerical simulation

Fluent CFD software was used to solve the numerical simulation in FSP. The finite volume method (FVM) combined CATIA and ICEM surf software was utilized to construct the welded joint model. The temperature field and flow field of FSP precursor were employed to study the joint quality. A particle tracing method was proposed for analyzing the flow of TiH₂ and Al₂O₃ powder in preformed billet. A schematic illustration of FSP process and its geometrical model features for numerical simulation was shown in Fig. 4. In order to simplify the FSP model, the effects of tool shoulder concavity and tool tilt angle were ignored. The calculated domain size of the model was 80 mm × 50 mm, and two 7075 aluminum plates (2 mm × 1.5 mm) were superimposed. The grid division process was carried out in ANSYS ICEM CFD software. The

grid size of the model was set as 2 mm, and the model grid division was shown in Fig. 5.

The flow of TiH₂ and Al₂O₃ powder in the preformed billet was analyzed by particle tracing method during FSP. The tracking particles were added to the CFD model as part of the pre-simulation setup. Since the particle flow direction was opposite to the processing direction, 630 tracer particles were evenly distributed in the ZY plane which was in front of the axis of the agitator pin, as shown in Fig. 6.

Based on model prediction, the workpiece material was treated as a non-Newtonian fluid. The general governing equations for the heat transfer and the material flow for incompressible single-phase fluid were used in this work. The conservation equations of mass and momentum could be shown as follows [22]:

$$\frac{\partial \rho}{\partial t} + \nabla \cdot \rho \vec{v} = 0 \tag{1}$$

$$\frac{\partial \rho \vec{v}}{\partial t} + \nabla \cdot (\rho \vec{v} \vec{v}) = -\nabla P + \nabla \cdot (\mu (\nabla \vec{v} + \nabla \vec{v}^T)) \tag{2}$$

where ρ was the fluid density, μ was the fluid viscosity, p was the pressure, \vec{v} was the fluid velocity and t was the flow time, respectively.

In different coordinate axes, the conservation equations of mass and momentum were given as:

Fig. 3 Schematic illustrations of closed-cell Al foam precursor by multipass FSP

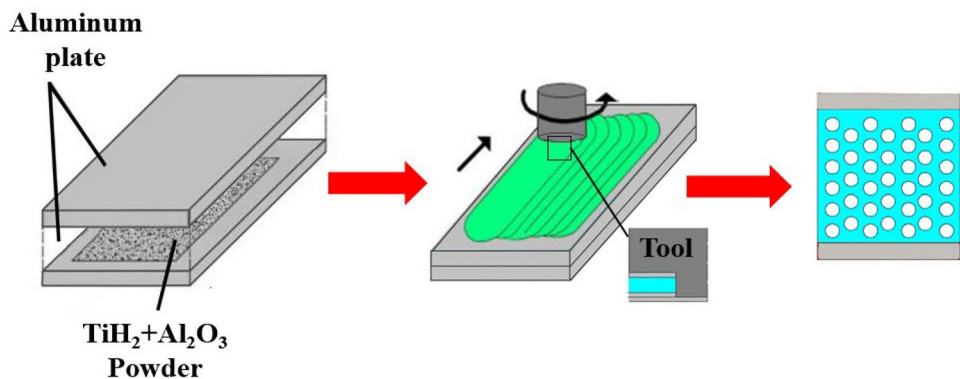
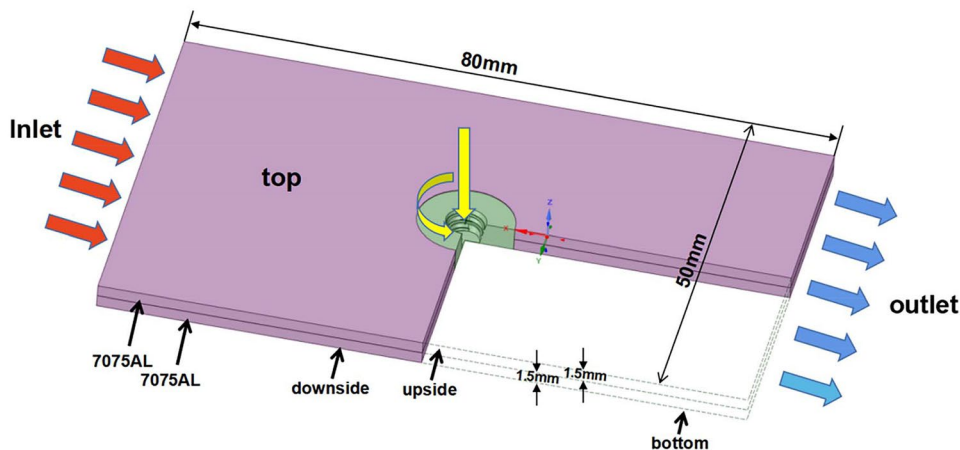


Fig. 4 A schematic of FSP process and its corresponding geometrical model



$$\begin{aligned} \frac{\partial (\rho u)}{\partial t} + \rho \left((u - u_{weld}) \frac{\partial u}{\partial x} + \frac{\partial v}{\partial y} + \frac{\partial w}{\partial z} \right) \\ = \frac{\partial p}{\partial x} + \frac{\partial}{\partial x} \left(\mu \frac{\partial u}{\partial x} \right) + \frac{\partial}{\partial y} \left(\mu \frac{\partial u}{\partial y} \right) + \frac{\partial}{\partial z} \left(\mu \frac{\partial u}{\partial z} \right) \end{aligned} \quad (3)$$

$$\begin{aligned} \frac{\partial (\rho v)}{\partial t} + \rho \left((u - u_{weld}) \frac{\partial u}{\partial x} + \frac{\partial v}{\partial y} + \frac{\partial w}{\partial z} \right) \\ = \frac{\partial p}{\partial x} + \frac{\partial}{\partial x} \left(\mu \frac{\partial v}{\partial x} \right) + \frac{\partial}{\partial y} \left(\mu \frac{\partial v}{\partial y} \right) + \frac{\partial}{\partial z} \left(\mu \frac{\partial v}{\partial z} \right) \end{aligned} \quad (4)$$

$$\begin{aligned} \frac{\partial (\rho w)}{\partial t} + \rho \left((u - u_{weld}) \frac{\partial u}{\partial x} + \frac{\partial v}{\partial y} + \frac{\partial w}{\partial z} \right) \\ = \frac{\partial p}{\partial x} + \frac{\partial}{\partial x} \left(\mu \frac{\partial w}{\partial x} \right) + \frac{\partial}{\partial y} \left(\mu \frac{\partial w}{\partial y} \right) + \frac{\partial}{\partial z} \left(\mu \frac{\partial w}{\partial z} \right) \end{aligned} \quad (5)$$

where the numbers $x, y,$ and z were the $x-, y-,$ and z -coordinates, and u, v, w were the material velocity projections of the fluid material on the $x, y,$ and z coordinates, and u_{weld} was the tool travel velocity.

In this simulation, the material flow process involved heat generation and heat dissipation. Therefore, the fluid flow system should meet the law of conservation of energy:

$$\begin{aligned} \frac{\partial (\rho C_p w)}{\partial t} + \rho C_p \left((u - u_{weld}) \frac{\partial T}{\partial x} + v \frac{\partial T}{\partial y} + w \frac{\partial T}{\partial z} \right) \\ = k \left(\frac{\partial^2 T}{\partial x^2} + \frac{\partial^2 T}{\partial y^2} + \frac{\partial^2 T}{\partial z^2} \right) + S_v \end{aligned} \quad (6)$$

where C_p was the specific heat capacity of the material, T was the absolute temperature, k was the thermal conductivity, and S_v was the viscous dissipation caused by the plastic deformation of the shear layer during the plastic flow of the material.

Fig. 5 Mesh view of the cylindrical threaded pin wall embedded in the plates

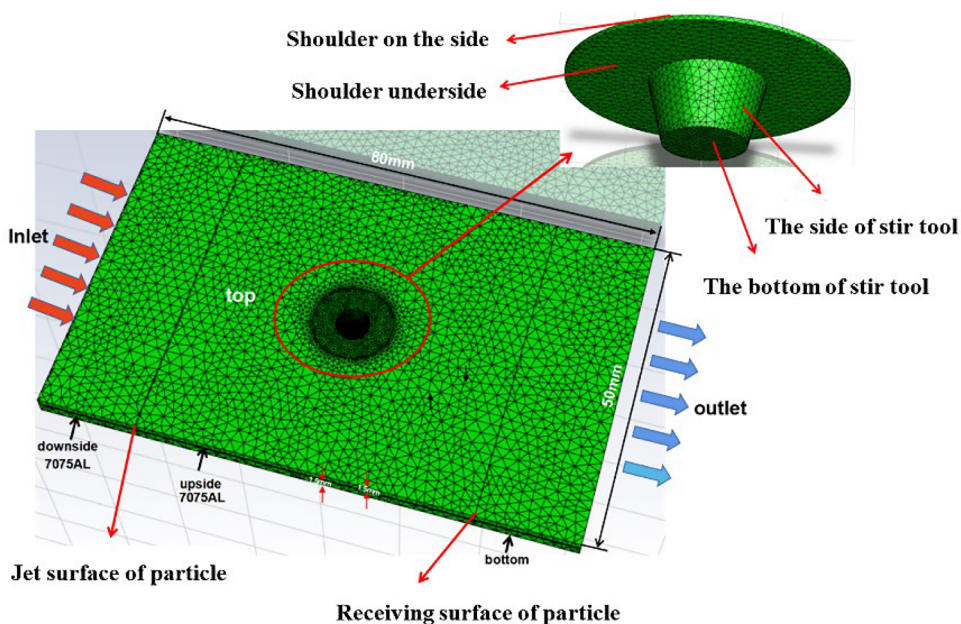
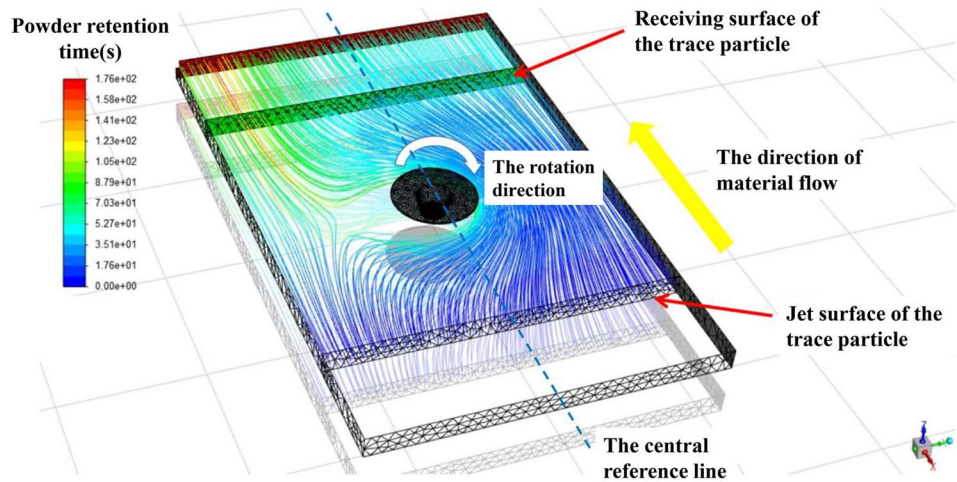


Fig. 6 Tracking powder process diagram



According to the reference [22], the energy conservation equation was given as follows:

$$\frac{\partial \rho H}{\partial t} + \nabla \cdot (\rho \vec{v} H) = \nabla \cdot (k \nabla T) + S_v \tag{7}$$

$$H = \int_{T_{ref}}^T C_p dT \tag{8}$$

where H is the enthalpy, k is the thermal conductivity, T is the Kelvin temperature, S_v is the spatial source term of the heat generation, C_p is the specific heat, and T_{ref} is the reference temperature.

The velocity and thermal boundary conditions were the main considerations in the simulation of FSP. Its velocity boundary condition can be expressed as:

$$\begin{cases} lu = (1 - \delta)(\omega r \sin\theta - V_{weld}) \\ v = (1 - \delta) \omega r \cos\theta \\ w = \frac{\psi \omega}{2\pi} \end{cases} \tag{9}$$

where u , v , and w were the relative speeds in x , y , and z directions respectively, and ψ was the stirring pin thread.

The δ represented the slip rate which was used to describe the contact state between the tool and workpiece, as shown below.

$$\delta = 0.31 \times \exp\left(\frac{\omega r}{1.87}\right) - 0.026 \tag{10}$$

Fig. 7 Macromorphology of the foam precursor with welding spacing of 3 mm



where r represented the distance from the elemental area to the tool axis and ω was the rotational speed of the tool.

The thermal boundary condition could be expressed as:

$$-k \frac{\partial T}{\partial z} = \epsilon_r \delta_r (T^4 - T_0^4) + h_{Al} (T - T_0) \tag{11}$$

where k is the thermal conductivity of the material, ϵ_r is the thermal radiation coefficient, δ_r is the Stefan-Boltzmann constant, T_0 is the ambient temperature, and h_{Al} is the convective heat transfer coefficient whose value was 25.0 W/(m²·K) [23].

To calculate heat input per unit length, the heat index (HI) value was proposed as follows [24]:

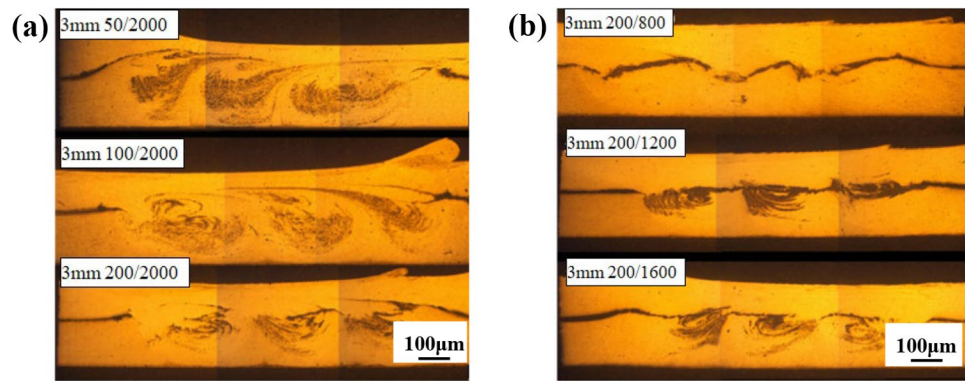
$$HI = \frac{\omega^2}{v \times 10^4} \tag{12}$$

4 Results and analysis

4.1 The effect of different process parameters on the microstructure of closed-cell Al foam precursor

Figure 7 illustrates the macromorphology of the foam precursor with welding spacing of 3 mm. It can be seen that the surface microstructure is smooth and compact. There is no defect such as microholes, cracks, and flash on sample surface. Figure 8 shows the cross-sectional morphologies of closed-cell Al foam precursor at the different travel speeds. The travel speeds are varied from 50, 100, and 200 mm/min in Fig. 8a. According to

Fig. 8 Cross-section morphologies of closed-cell Al foam precursor at different process parameters



the morphology of the Al foam precursor in Fig. 8a, the entire sample retains a good surface. The typical “onion ring” morphology appears on all sample cross sections at the different travel speeds at a constant rotation speed 2000 r/min.

When the tool travel speed is 50 mm/min and the rotating speed is 2000 r/min, the mixing powder in the aluminum matrix is subjected to the strong rotating of the stirring pin. Simultaneously, sufficient plastic deformation and material flow occurs in the stirring zone. Therefore, the powder ring in the stirring zone is continuous and uniform. However, the width of stirring zone decreases gradually with the increase of the tool travel speed. When the tool travel speed increases from 50 to 200 mm/min, the heat index value decreases from 8 to 2 kJ/mm. The plastic deformation and fluidity of the material are reduced, and the powder ring becomes narrow. This is because that the high heat index values of 2–8 kJ/mm are obtained, when the rotation speed is 2000 r/min. The high heat input values promote the fluidity of molten pool.

Figure 8b illustrates the cross-sectional morphologies of closed-cell Al foam precursor at the different rotating speeds. The rotating speeds are 800, 1200, and 1600 r/min, respectively. It can be seen that the morphology is highly sensitive to change in different rotating parameter [21]. The foaming agent TiH_2 and stabilizer Al_2O_3 powder in the interlayer are not mixed evenly with the aluminum matrix at the rotational speed of 800 r/min and 1600 r/min. There is obvious stratification between the powder and the aluminum matrix. This is because when the rotation speed changes from 800 to 1600 r/min, the low heat input values of 0.32–1.28 kJ/mm are obtained. The molten pool temperature is low and the fluidity of materials is poor. With increasing the rotating speed of the tool shoulder, more material generates flow in the counter clockwise direction. The mixed powder is gradually integrated into the aluminum matrix, and the radius of the mixing area gradually increases.

Figure 9 shows the SEM morphology and EDS analysis of the mixing area of closed-cell Al foam precursor at the tool travel speed of 50 mm/min and rotational speed of 2000 r/min. It can be seen that the gray area is Al matrix, and the small white particles are TiH_2 . The Al_2O_3 powder as gray

cloudlike region is distributed almost uniformly in the precursor. In addition, the frictional force has resulted in the uniform flow of stir zone. The experimental results prove that TiH_2 and Al_2O_3 mixed powders can be uniformly mixed in aluminum matrix by high-speed rotation of stirring pin and multipass FSP.

4.2 The effect of different foaming time on the microstructure of closed-cell Al foam

In order to achieve foaming of the FSP plates, the precursors at the tool travel speed of 50 mm/min and rotational speed of 2000 r/min are foamed at 680 °C for different time. The samples are easy to be oxidized, so argon is used as a protective gas.

Figure 10 shows the cross-section photographs of closed-cell Al foams fabricated at 680 °C. The micrographs illustrate the qualitative assessment of the cellular structures evolution for Al foam precursor at different foaming time. When the foaming time is 60 s, the foaming effect is poor. There is more than 90% of the area without

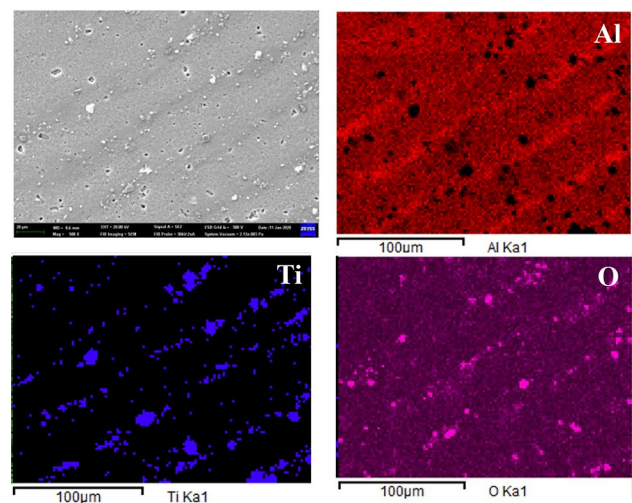
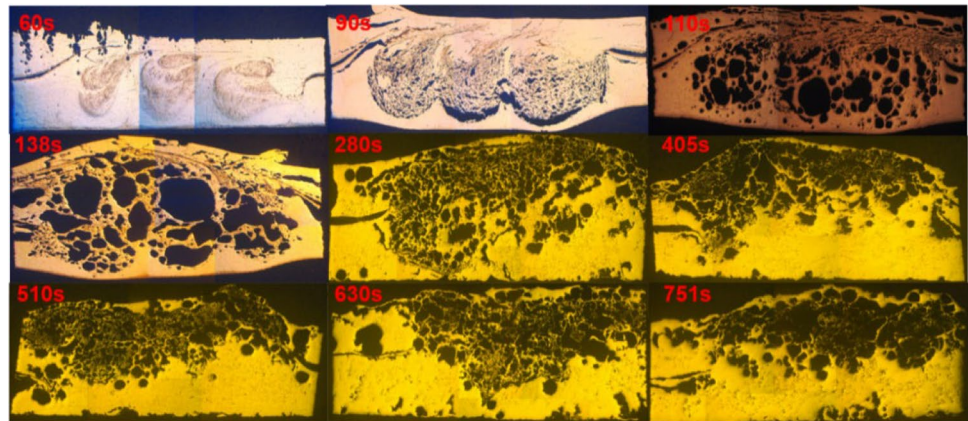


Fig. 9 The cross-section SEM image and the EDS maps of the relevant elements in the Al foam precursor with the travel speed of 50 mm/min and rotational speed of 2000 r/min

Fig. 10 Morphology of cross section of closed-cell Al foam after foaming for different time at 680 °C



foaming. Very small pores appear in the processing area of the precursor after 90 s, and simultaneously the number of pores at the bottom of the processing area is greater than that at the top. With the extension of the foaming time, part of TiH_2 powder begins to release gas, and the pore size in the processing area gradually increases.

When the foaming time is 110 s, the expansion rate of the whole foam increases rapidly, and the bubble pores at the bottom tends to be round and the pore structure is uniform in Fig. 10. At 138 s, TiH_2 powder completely releases the gas, and the pores are distributed in the whole section. However, the size of the pores is not uniform. Some uniform round pores are connected with each other to form the whole pores. In the range of 280–751 s, the circular pores appear collapse due to the further extension of the foaming time. In addition, partially collapsed pores gradually shrink and merge at the bottom. The results show that the foaming process of the precursor starts from the bottom and then goes up. Finally, the pores merge with each other and gradually expansion. The bottom pores appear to collapse into compaction.

4.3 Numerical simulation of temperature field of closed-cell Al foam precursor in FSP process

Figure 11 presents numerical simulation of the temperature distribution at top surface of the workpiece at different rotating speeds with a constant travel speed of 50 mm/min. The process parameters of the simulation were selected with 800, 1200, 1600, and 2000 r/min, respectively. As it can be seen, the processing temperature peak appears near the stirring pin, which is distributed in a “bowl shape.” In addition, the temperature decreases gradually with the increase of the distance between the stirring pin center. The closed-cell Al foam precursor in the weld line area undergoes higher velocity and deformation than in the external side.

At the same time, the rotating speed has great influence on the temperature field of the foam precursor during the FSP. When the rotating speed increases from 800 to 2000 r/min, the temperatures increase by 130 °C. In particular, when the rotating speed is 2000 r/min, the peak temperature at the stirring pin reaches 491 °C. It indicates that the

Fig. 11 Numerical simulation of the temperature distribution at top surface of the workpiece at different rotating speeds with a constant tool travel speed of 50 mm/min

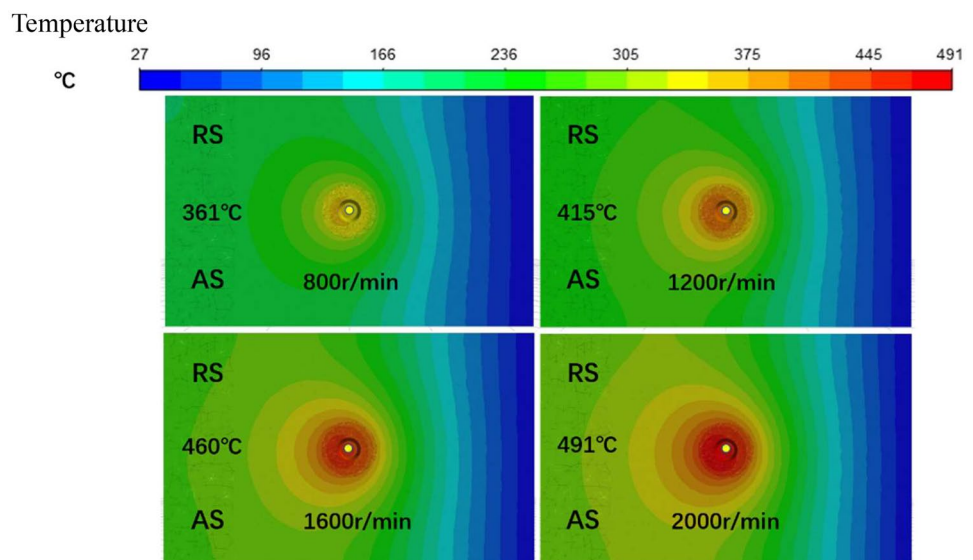
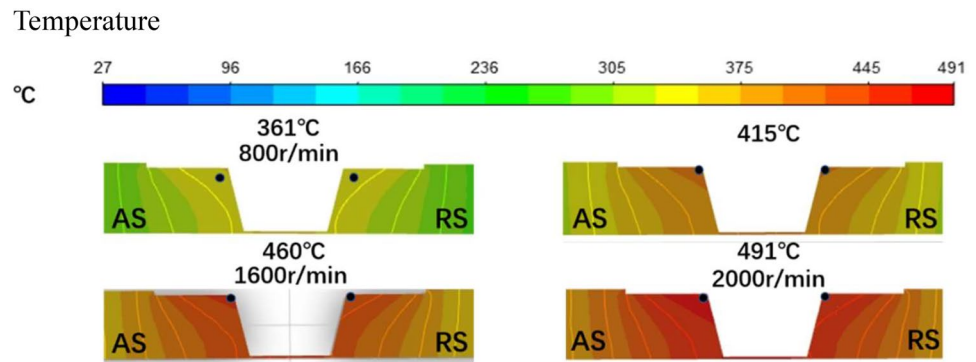


Fig. 12 The simulated temperature field of transverse cross-section of Al foam precursor joint at different rotational speeds with a constant tool travel speed of 50 mm/min



processing temperature of the stirring pin increases gradually with the increase of rotating speed.

Figure 12 shows the simulated temperature field of transverse cross-section of the precursor at different rotating speeds with a constant tool travel speed of 50 mm/min. It can be seen that the variation of temperature is found to be different on the advancing (AS) and the retarding sides (RS). The temperature on the advancing side is higher than that on the retreating side. Simultaneously, the profile of the temperature distribution is non-symmetric on both sides of the stirring pin, which is affected by changing the FSP processing parameters. The peak temperature is obtained near the tool shoulder. The results prove that the amount of heat generation mainly comes from the friction between the shoulder and workpieces.

In the FSP, the high-temperature plastic metal in the viscoelastic zone is extruded to the backward side by the rotation of stirring pin, which causes sufficient plastic deformation and flow of the metal in the processing zone. When the rotational speed is 800 r/min, the simulated temperature field of the cross section of the joint is only 361 °C. The main reason is that the friction between the stirring pin and the sample generates less heat. The thermal convection between the workpiece and the surrounding environment is small, which makes it easy to stratify in both the upper and lower plates as shown in Fig. 8. The interface temperatures of the joint increase rapidly with the increase of the rotation speed. When the rotational speed is 2000 r/min, more heat is generated and the peak temperature value is obtained for 491 °C. The material in this temperature range is softened and reaches the plasticized state under the extrusion and shearing action of the stirring pin.

Figure 13 illustrates a comparison between the experimental temperature result and the numerically calculated one in FSP. The time–temperature (t - T) relationship curve during the experiment is extracted from the infrared thermal imager, when the travel speed is 50 mm/min and the rotational speed is 2000 r/min. At the same time, numerical simulation of the temperature distribution under the same conditions is obtained. The result shows that the simulation value matches well with experimental one.

4.4 Numerical simulation of material flow field of closed-cell Al foam precursor in FSP process

Figure 14 illustrates the numerical simulation of material flow of Al foam precursor at 800, 1200, 1600, and 2000 r/min with tool travel speed of 50 mm/min, respectively. It can be seen that material flow occurs mainly on the upper surface. It is because that the tool shoulder plays a leading role in the plastic material movement. At the same time, the material flow velocity on the retreating side (RS) is slightly higher than that on the advancing side (AS), which is consistent with the literature reported by Morisada et al. [25]. At the pin side surface, due to the action of the stirring pin, the material moves downward and reflows when it reaches the bottom, and the trajectory is a semicircular motion. Therefore, the materials in the weld area undergo multiple rotation and extrusion because of the forced driving effect of the stirring pin.

Firstly, the aluminum matrix at the outer edge of the tool shoulder is preferred to soften due to the frictional shear force of FSP process, and a plastic softening zone is formed.

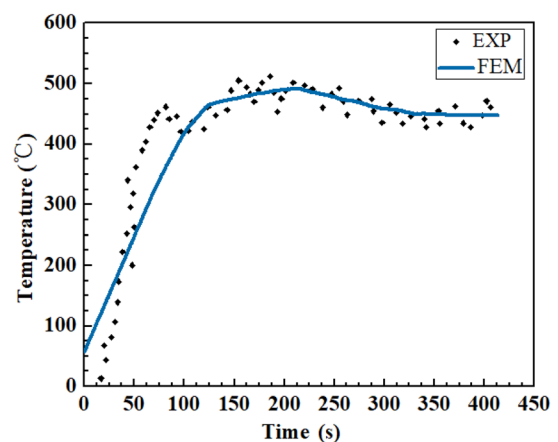
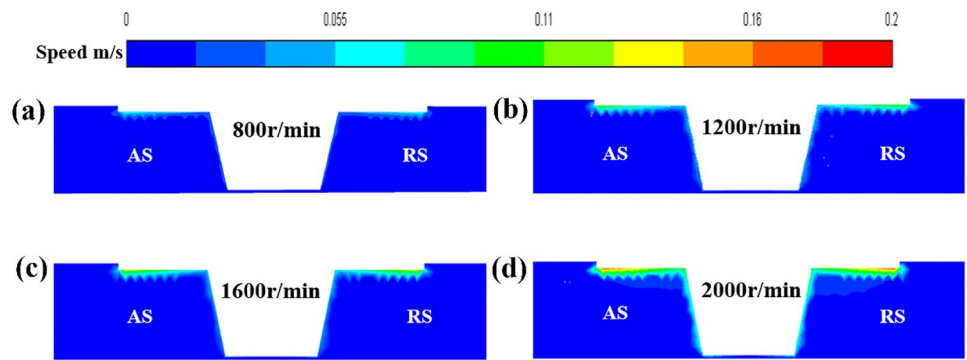


Fig. 13 A comparison between experimental result and finite element analysis (FEA) result at rotational speed of 2000 r/min with a constant tool travel speed of 50 mm/min

Fig. 14 Numerical simulation of material flow of Al foam precursor at different rotation speeds 800, 1200, 1600, and 2000 r/min with a constant tool travel speed 50 mm/min



Then most of the softened layer particles are spiraled from the advancing side to the retreating side due to the intense stirring action of the pin. Moreover, the linear velocity of the shoulder decreases with increasing the distance from the axis. The plastic flow of metal in the vicinity of the shoulder area increases gradually with increasing rotational speed. The material flow velocity of the outermost edge of the tool shoulder increases by 1.5 times, when the rotating speed increases from 800 to 2000 r/min. The powder mixing ring has a large diameter, which is consistent with the experimental result in Fig. 8.

Figure 15 shows the heat flow at the tool-workpiece interface for different rotation speeds 800, 1200, 1600, and 2000 r/min. The magnitude of heat flow increases gradually from the center of the tool axis to the outer edge. In addition, due to the effective contact area of the stirring pin, the heat flow is distributed periodically at pin side-workpiece interface. It is evident that the heat flow is proportional to the relative velocity. The maximum occurs at the edge of the

tool shoulder. Simultaneously, the heat flow value increases gradually with the increase of rotation speed. Especially the heat flow increases 1.5 times when the rotating speed increases from 800 r/min to 2000 r/min. The results show that more heat is generated at the tool shoulder and effectively improve material flow.

Figure 16 shows the streamlines and velocity field of the simulated material flow near the tool at different rotation speeds with a constant tool travel speed 50 mm/min. It can be seen that the material flow in the stirring zone increases as the rotation speed increases. Since the rotation direction of the tool is counter clockwise, the softened material under the extrusion action gradually extends outward. Simultaneously, the material flow region is expanded as the speed of rotation increases. The direction of plastic flow of weld metal is consistent with the rotation direction of the tool. When the rotating speed is between 800 and 1200 r/min, the backward side metal has not been filled due to the low processing heat, and the plastic flow capacity of the material is poor. The

Fig. 15 Calculated heat flow at tool-workpiece interface for different rotation speeds 800, 1200, 1600, and 2000 r/min

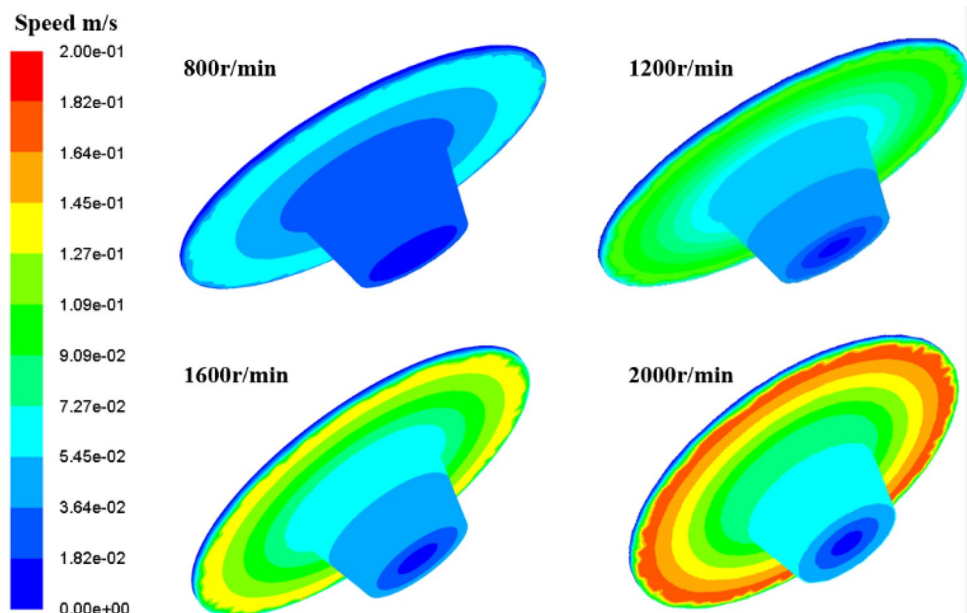
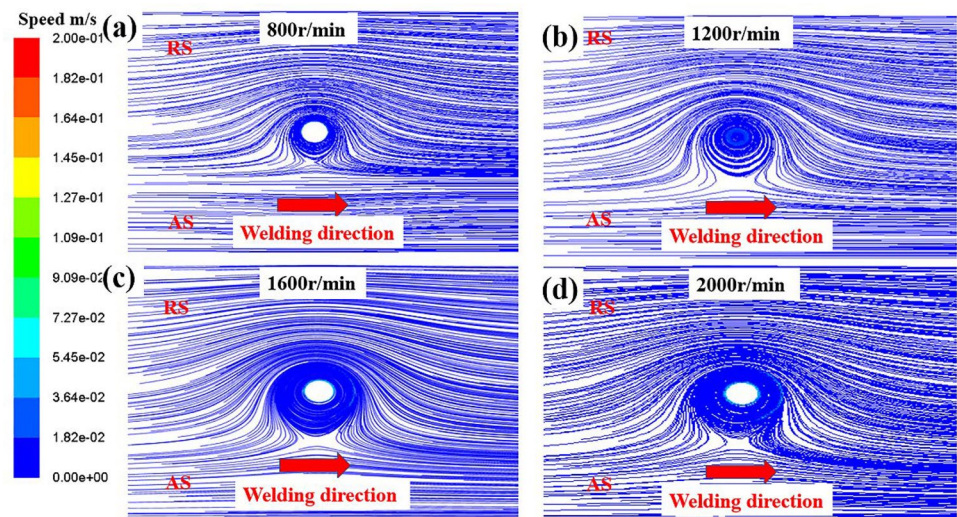


Fig. 16 Streamlines and velocity field of joint interface at different rotation speeds 800, 1200, 1600, and 2000 r/min with a constant tool travel speed 50 mm/min

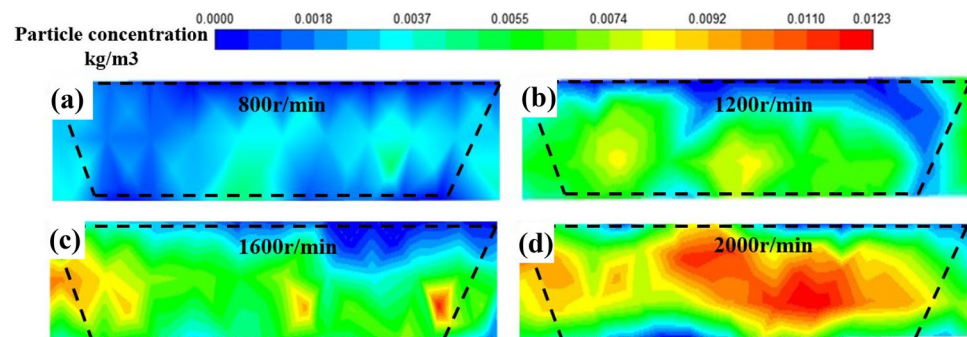


plastic flow capacity of the material is improved gradually with the increase of rotation speed. Especially when the tool travel speed reaches 2000 r/min, the gap caused by rotation is completely filled at the forward side. The formability of the joint interface is improved.

4.5 Numerical simulation analysis of tracking particles in closed-cell Al prefabricated foam

Figure 17 shows the tracking particle concentration of joint interface at different rotation speeds. The tracking particles are initially arranged on the processing area during the simulation. In the initial stage, the Al matrix is not softened and the particles are mainly squeezed by the stirring pin. Then, a plastic softening layer is formed and the particles start to flow under the action of the stirring pin. As can be seen from the figure, the numerical simulation of tracking particles presents blue areas, covering the whole preformed powder ring in Fig. 17a. Simultaneously, the total particle concentration gradually increases with the increase of the rotational speed. Due to obvious stratification at the joint interface, the highest concentration of powder tracking particles is 0.0096 kg/m^3 at the rotation speed of 800 r/min and the travel speed of 50 mm/min.

Fig. 17 Tracking particle concentration of joint interface at tool travel speed of 50 mm/min and different rotation speeds: **a** 800 r/min, **b** 1200 r/min, **c** 1600 r/min, **d** 2000 r/min



When the travel speed increases from 50 to 200 mm/min with a consistent rotation speed of 2000 r/min, the heat input value is significantly reduced from 8 to 2 kJ/mm. At the same time, when the rotating speed increases from 800 to 2000 r/min, the maximum flow velocity of material in the tool shoulder increases by 1.5 times. The highest concentration of powder tracking particles increases separately to 0.0096 kg/m^3 and 0.0137 kg/m^3 , when the rotation speed increases from 800 to 2000 r/min in Fig. 17b, c. In addition, the blue area is gradually replaced by the green area in the numerical simulation. When the rotation speed is 2000 r/min, the highest concentration of powder tracing particles is 0.0123 kg/m^3 in Fig. 17d. The red area with high particle concentration is gradually increased by numerical simulation, which almost covers the precursor area.

Figure 18 illustrates the forming limit curves of aluminum foam precursor at different deformation temperatures. The cupping test value of 7075 aluminum alloy sheet is 27 mm at room temperature. Although the temperature increases continuously, the cupping test value does not fluctuate greatly in Fig. 18b. As for the aluminum foam precursor, the cupping test value of the sample is low at room temperature, which shows obvious brittleness characteristics. The plasticity of the sample is enhanced with the increase of the

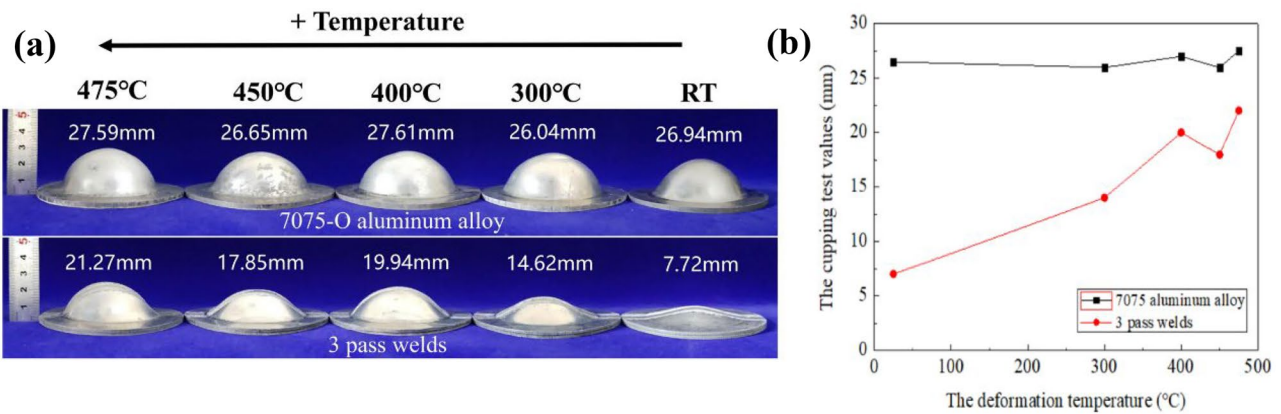


Fig. 18 The cupping test values of foam specimens at different deformation temperatures

temperature. The cupping test values of the aluminum foam precursor increase obviously with the increase of deformation temperature. When the deformation temperature reaches 475 °C, the maximum cupping test value of the precursor is 21.27 mm, which is 2.7 times higher than that of room temperature value.

5 Discussion

The numerical simulation results show that there are great differences in temperature field distribution and plastic flow of stirring pin at different processing parameters. The temperature on the advancing side is significantly higher than that on the retreating side. Therefore, the plastic flow on the advancing side is much better than that on the retreating side.

In the FSP, the 7075-O aluminum alloy sheet is used instead of aluminum powder, which can effectively avoid and reduce powder agglomeration and crack defects. The processing heat mainly comes from the tool shoulder of the stirring pin due to friction between the stirring pin and aluminum matrix. In addition, during the high-speed rotation of the stirring pin, the maximum flow velocity appears at the outer edge of the tool shoulder, and the aluminum matrix at the outer edge of the tool shoulder is softened preferentially. With the prolonging of processing time, the softening zone of aluminum matrix gradually increases, and the material reaches the state of plastic flow. As the stirring pin moves forward, the high temperature plastic metal is continuously extruded from the advancing side to the retreating side by the rotating motion of the stirring pin, and the material in the processing zone has sufficient plastic deformation and flow. At the same time, the plastic flow capacity and the concentration of powder tracking particles can be effectively improved by increasing the rotating speed of the stirring pin.

When the tool travel speed is 50 mm/min and the rotation speeds is 2000 r/min, the temperature field and heat flow of the outer edge of the contact surface between the tool shoulder and substrate are the maximum and the highest values are 491 °C and 6.20×10^6 W/m², respectively. In addition, the heat flow on the surface of the tool shoulder decreases with the decrease of the radius from the shoulder center. When the rotating speed of the stirring pin increases from 800 to 2000 r/min, the flow speed at the outer edge of the tool shoulder increases by 59.96%, and the highest concentration of powder tracking particles increases by 28.1%, which is beneficial to the uniformity of the welded joint. Therefore, the simulation results reveal that the FSP leads to a better powder distribution, which is consistent with the experimentally result acquired.

In the process of the cupping test of Al foam precursor, the cupping test value of the sample is low at room temperature, which shows obvious brittleness characteristics. The plasticity of Al foam precursor is enhanced with the increase of deformation temperature. It shows high formability as deformation temperatures above 400 °C, the maximum cupping test value of the precursor is 21.27 mm at 475 °C, which is closed to that of the 7075-O sheet. This is largely due to the thermal activation relaxation in the grain and grain boundary [26, 27]. As a result, the grain boundary slipped, dynamic recovery and dynamic recrystallization gradually begin with the increase of temperature. After the progress of thermal activation, the plasticity of the precursors increases sharply as shown in Fig. 18.

6 Conclusions

In the paper, the closed-cell Al foams are successfully obtained by using FSP and post-weld foam treatment. The influence of process parameters on microstructures of closed-cell Al foam are evaluated by experiment and

numerical simulation. The following conclusions can be drawn:

1. Sufficient plastic deformation and flow occur in the processing zone when the travel speed is 50 mm/min, and the rotating speed is 2000 r/min. TiH₂ and Al₂O₃ mixed powders can be uniformly mixed in aluminum sheet by 3 passes FSP.
2. The numerical simulation analysis shows that the temperature decreases gradually with the increase of the distance between the stirring pin center. When the rotational speed is 2000 r/min, the peak temperature value is obtained for 491 °C. The highest concentration of powder tracing particles is 0.0123 kg/m³ at the travel speed of 50 mm/min and the rotating speed of 2000 r/min, which indicates that mixed powders can be uniformly distributed. This is consistent with the experimental result.
3. In the foaming process at 680 °C, the foam pores first appear at the bottom and then expand upwards with the extension of the foaming time. When the foaming time is 110 s, the expansion rate of the whole foam increases rapidly, and the pores with highly spherical are homogeneously distributed.
4. As for the aluminum foamed preform, the plasticity of the Al foam precursor is enhanced with the increase of the deformation temperature. The maximum cupping test value of the precursor is 21.27 mm, which is 2.7 times higher than that of room temperature value. It shows high formability as deformation temperatures above 400 °C, which is closed to that of the 7075-O sheet.

Author contribution Qiu Pang conceived the theory, designed experiments, and wrote the paper. Zhengjian Wu helped with the experiments. Prof. Zhili Hu initialized and supervised the research.

Funding This work was supported by the Hubei Key Laboratory of Advanced Technology for Automotive Components fund (XDQCKF2021007), National Natural Science Foundation of China (51775397, 52075400, 51805393), 111 Project (B17034), Major Program of Science and Technology Program of Hubei Province (2020BAB140), and Innovative Research Team Development Program of Ministry of Education of China (IRT17R83).

Declarations

Ethics approval The authors conducted their work from research proposal to publication in line with best practices and codes of conduct of relevant professional bodies.

Consent to participate All authors have approved to participate.

Consent for publication The manuscript is approved by all authors for publication.

Conflict of interest The authors declare no competing interests.

References

1. Banhart J (2013) Light-metal foams—history of innovation and technological challenges. *Adv Eng Mater* 15:82–111
2. Gibson LJ, Ashby MF (1997) Cellular solids: structure and properties. Cambridge University Press, Cambridge New York
3. Nowacki J, Sajek A (2019) Trends of joining composite AlSi-SiC foams. *Adv Mater Sci* 19:70–81
4. Wan T, Liu Y, Zhou CX, Chen X, Li YX (2021) Fabrication, properties, and applications of open-cell aluminum foams: A review. *J Mater Sci Technol* 62:11–24
5. Su BY, Huang CM, Sheng H, Jang WY (2018) The effect of cell-size dispersity on the mechanical properties of closed-cell aluminum foam. *Mater Charact* 135:203–213
6. Roohi AH, Naeini HM, Gollo MH, Soltanpour M, Bruschi S, Ghiotti A (2018) Forming of closed-cell aluminum foams under thermal loadings: experimental investigation. *Int J Adv Manuf Technol* 95:3919–3928
7. Zhang M, Chen CJ, Brandal G, Bian D, Yao YL (2016) Experimental and numerical investigation of laser forming of closed-cell aluminum foam. *J Manuf Sci E* 138:021006
8. Hangai Y, Kawato D, Ando M, Ohashi M, Morisada Y (2020) Nondestructive observation of pores during press forming of aluminum foam by X-ray radiography. *Mater Charact* 170:110631
9. Shiomi M, Fukaya T (2014) Forming of aluminum foams by using rotating mold. *Procedia Engineering* 81:664–669
10. Chen SG, Chen HB, Sun ZZ, Li RY, He WF (2014) The U-bending forming of aluminum foam sandwich panels. *Appl Mech Mater* 477–478:1432–1439
11. Nowacki J, Sajek A (2019) Trends of joining composite AlSi-SiC foams. *Adv Mater Sci* 19(1):70–82
12. Janeczek A, Tomkow J, Fydrych D (2021) The influence of tool shape and process parameters on the mechanical properties of AW-3004 aluminium alloy friction stir welded joints. *Materials* 14(12):3244
13. Tamadon A, Pons DJ, Sued K, Clucas D (2021) Internal flow behaviour and microstructural evolution of the bobbin-FSW welds: thermomechanical comparison between 1xxx and 3xxx aluminium grades. *Adv Mater Sci* 21(2):40–64
14. Lotfi AH, Nourouz S (2021) Predictions of the optimized friction stir welding process parameters for joining AA7075-T6 aluminum alloy using preheating system. *Int J Adv Manuf Technol* 73(9–12):1717–1737
15. Heidarzadeh A, Mironov S, Kaibyshev R, Cam G, Simar A, Gerlich A (2021) Friction stir welding/processing of metals and alloys: a comprehensive review on microstructural evolution. *Prog Mater Sci* 117:100752
16. Azizieh M, Pourmansouri R, Balak Z, Kafashan H, Mazaheri M, Kim HS (2017) The application of friction stir processing to the fabrication of magnesium-based foams. *Arch Metall Mater* 62(4):1957–1962
17. Papantoniou IG, Kyriakopoulou HP, Pantelis DI, Athanasiou-Ioannou A, Manolakos DE (2018) Manufacturing process of AA5083/nanogamma Al₂O₃ localized composite metal foam fabricated by friction stir processing route (FSP) and microstructural characterization. *J Mater Sci* 53(5):3817–3835
18. Yamamura K, Kawada N, Nishihara T (2010) Formation of local metallic foam of aluminum alloy using friction stir processing. *J Jpn I Met* 74:55–60
19. Shandley R, Maheshwari S, Siddiquee AN, Mohammed SMAK, Chen DL (2020) Foaming of friction stir processed Al/MgCO₃ precursor via flame heating. *Mater Res Express* 7(2):026515
20. Pang Q, Hu ZL, Song JS (2019) Preparation and mechanical properties of closed-cell CNTs-reinforced Al composite foams by friction stir welding. *Int J Adv Manuf Technol* 103(5–8):1036–1042

21. Hangai Y, Takada K, Fujii H, Aoki Y, Aihara Y, Nagahiro R (2020) Foaming of A1050 aluminum precursor by generated frictional heat during friction stir processing of steel plate. *Int J Adv Manuf Technol* 85(2):84–87
22. Chen GQ, Li H, Wang GQ, Guo ZQ, Zhang S, Dai QL, Wang XB, Zhang G, Shi QY (2018) Effects of pin thread on the in-process material flow behavior during friction stir welding: a computational fluid dynamics study. *Int J Mach Tool Manu* 124:12–21
23. Kadian AK, Biswas P (2015) A comparative study of material flow behavior in friction stir welding using laminar and turbulent models. *J Mater Eng Perform* 24:4119–4127
24. Mishra RS, Ma ZY (2005) Friction stir welding and processing. *Mater Sci Eng R-Rep* 50:1
25. Morisada Y, Fujii H, Kawahito Y, Nakata K, Tanaka M (2011) Three-dimensional visualization of material flow during friction stir welding by two pairs of X-ray transmission systems. *Scr Mater* 65:1085–1088
26. Appel F, Lorenz U, Oehring M, Sparka U, Wagner R (1997) Thermally activated deformation mechanisms in micro-alloyed two-phase titanium amminide alloys. *Mater Sci Eng A* 233:1–14
27. Imayev VM, Imayev RM, Salishchev GA (2000) On two stages of brittle-to-ductile transition in TiAl intermetallic. *Intermetallics* 8:1–6

Publisher's Note Springer Nature remains neutral with regard to jurisdictional claims in published maps and institutional affiliations.